

# Star formation histories of resolved galaxies. I. The method

Emma E. Small<sup>1\*</sup>, David Bersier<sup>1</sup> and Maurizio Salaris<sup>1</sup>

<sup>1</sup>*Astrophysics Research Institute, Liverpool John Moores University, Egerton Wharf, Birkenhead, CH41 1LD, UK*

31 October 2012

## ABSTRACT

We present a new method to determine the star formation and metal enrichment histories of any resolved stellar system. This method is based on the fact that any observed star in a colour-magnitude diagram will have a certain probability of being associated with an isochrone characterised by an age  $t$  and metallicity  $[\text{Fe}/\text{H}]$  (i.e. to have formed at the time and with the metallicity of that isochrone). We formulate this as a maximum likelihood problem that is then solved with a genetic algorithm. We test the method with synthetic simple and complex stellar populations. We also present tests using real data for open and globular clusters. We are able to determine parameters for the clusters ( $t$ ,  $[\text{Fe}/\text{H}]$ ) that agree well with results found in the literature. Our tests on complex stellar populations show that we can recover the star formation history and age-metallicity relation very accurately. Finally, we look at the history of the Carina dwarf galaxy using deep *BVI* data. Our results compare well with what we know about the history of Carina.

**Key words:** Hertzsprung-Russell and colour-magnitude diagrams – galaxies: evolution – Local Group – stars: evolution – methods: statistical

## 1 INTRODUCTION

There are two ways to approach the complex problem of galaxy evolution. One approach is to look at distant galaxies using integrated spectral energy distributions and determine broad properties of their star formation history and metal content. This provides a generalised view of star formation and galaxy evolution over cosmic time. However, it is difficult to match distant galaxies with their local counterparts.

Another approach is to resolve individual stars in nearby galaxies. The resulting colour-magnitude diagram (CMD) will contain information about the age and metallicity distributions of the stars. CMD analysis can provide a detailed picture about the star formation rate and metal enrichment history for each individual galaxy. However, it is difficult to draw general conclusions about galaxy evolution as this is essentially a case by case analysis.

This second technique has seen great progress in the last two decades and several methods have been devised to determine the star formation history (SFH) of nearby galaxies from CMDs. Most of these methods rely on creating synthetic CMDs to compare with the observed one using a merit function, usually a  $\chi^2$  or maximum likelihood technique. Variants of this method have been presented by e.g. Tolstoy & Saha (1996), Harris & Zaritsky (2001), Vergely et

al. (2002), Dolphin (2002), Aparicio & Hidalgo (2009) and de Boer et al. (2012).

Many of the methods use combinations of synthetic CMDs of “partial” stellar populations to reproduce different star formation histories. The stars of both observed and synthetic CMDs are grouped in boxes and the comparison is done on the numbers of stars in each box. This approach recovers both the star formation rate (SFR) and age-metallicity relation (AMR), which together, represents the SFH of the system. However, binning the CMD limits the resolution of the solution and introduces a subjective element into the method by choice of binning scheme [Aparicio & Hidalgo (2009) note that the binning scheme choice can affect results].

There is still a need for an objective method that doesn’t require parametrisation or binning. Hernandez et al. (1999) presented a non-parametric method that returns the star formation rate as a function of time, but assumes an age-metallicity relation. In a similar approach, Hernandez & Valls-Gabaud (2008) used a genetic algorithm to find the best-fitting isochrone for simple stellar populations, including distance and extinction into the fit. We approach this general problem in a way that is similar to Hernandez & Valls-Gabaud (2008), but extend it to derive any type of star formation and chemical enrichment history.

We represent a composite stellar population by a linear combination of isochrones, each with its own amplitude or weight. Therefore we are presenting a method that can

\* E-mail: ees@astro.livjm.ac.uk

be thought of as “multiple isochrone fitting”. This is a full maximum likelihood analysis that directly compares models with the observed data without the need for synthetic CMDs, simultaneously recovers SFR, AMR, distance and extinction, and properly weights each star in the likelihood function according to its measurement errors.

We present the method and its implementation in section 2. We test it on synthetic data for simple stellar populations in section 3 and on real data in section 4, where we look at several open and globular clusters. Section 5 shows how we can recover complex star formation histories and section 6 shows a comparison of our method with results obtained by other groups for the Carina dwarf spheroidal galaxy. We present a summary and conclusions in section 7.

## 2 MAXIMUM LIKELIHOOD METHOD

### 2.1 Likelihood Function

As discussed above, the stellar population content of any stellar system can be modeled as a linear combination of isochrones, each being characterised by its age and metallicity ( $t$ ,  $[\text{Fe}/\text{H}]$ )<sup>1</sup>. When reconstructing the SFH of the system, the specific problem is to use the information in the CMD in order to access the SFR as a function of time. Our approach is to calculate the relative probability that each star “originated” from a particular isochrone. This probability can be defined by the distance in magnitude space between an isochrone and the actual position of the star, accounting for the measurement errors. Formally, the problem then is to find the weight of each isochrone in the star formation history, i.e. the relative number of stars that each isochrone contributes to the CMD. We will build a likelihood function where the free parameters (i.e. the parameters that maximise the likelihood) are these isochrone weights.

We denote the magnitudes of a star  $j$  in two passbands as  $A_j$  and  $B_j$ . Corresponding theoretical magnitudes from isochrone  $i$  will be denoted  $A_{iM}$  and  $B_{iM}$  respectively. These  $A_{iM}$  and  $B_{iM}$  are shifted to account for the distance modulus and extinction of the observed system. The quantity

$$E(A_{ij}) = \frac{1}{2\pi\sigma_A} \exp \left[ -\frac{(A_j - A_{iM})^2}{2\sigma_A^2} \right] \quad (1)$$

represents the distance in magnitude  $A$  between the observed star  $j$  and a single point on isochrone  $i$ , assuming a gaussian error  $\sigma_A$  on  $A_j$ .  $\sigma_A$  is given by

$$\sigma_A = \sqrt{\sigma_{A,\text{phot}}^2 + \sigma_{A,\text{iso}}^2} \quad (2)$$

where  $\sigma_{A,\text{phot}}$  is the photometric error and  $\sigma_{A,\text{iso}}$  accounts for the differences in magnitude between two neighbouring isochrones. See sec 2.4 for the rationale behind the use of  $\sigma_{\text{iso}}$ .

Since the mass of star  $j$  is unknown, the probability function has to be an integral over all possible masses along

each isochrone. The probability will also need to be weighted by the relative number of stars along the isochrone, i.e. the IMF  $f(M)$ , and a function describing the observed photometric completeness  $c(A, B)$ . The relative probability  $p_{ij}$  that a given star  $j$  “belongs” to an isochrone  $i$  is

$$p_{ij} = \frac{1}{C_i} \int_{M_{il}}^{M_{iu}} E(A_{ij}) E(B_{ij}) c(A, B) f(M) dM \quad (3)$$

where  $M_{iu}$  and  $M_{il}$  are the upper and lower mass limits on the isochrone  $i$  and

$$C_i = \int_{M_{il}}^{M_{iu}} c(A, B) f(M) dM. \quad (4)$$

is a normalisation factor for the completeness and initial mass function.

In the above definition of the probability function we use two magnitudes,  $A$  and  $B$ . However this can easily be adapted to include 3 or more magnitudes. Since we consider the measurement of each magnitude to be independent, we can just include another term  $E(C_{ij})$  describing magnitude  $C$  and adjust the completeness function accordingly. The probability function for 3 magnitudes becomes:

$$p_{ij} = \frac{1}{C_i} \int_{M_{il}}^{M_{iu}} E(A_{ij}) E(B_{ij}) E(C_{ij}) c(A, B, C) f(M) dM \quad (5)$$

This will allow all photometric information for the data available for each star to be used to constrain the star formation history.

The next step in constructing our likelihood function is to determine the relative probability that a single star  $j$  belongs to a complex stellar population, which is represented by a linear combination of SSPs with different weights. The combined probability  $p_j$  is given by

$$p_j = \sum_{i=1}^{n_i} a_i p_{ij} \quad (6)$$

where  $a_i$  represents the weight of each isochrone and  $n_i$  is the total number of isochrones in the library. The weights are the relative number of stars each isochrone contributes to the CMD and are subject to the following constraints:

$$\sum_{i=1}^{n_i} a_i = 1 \quad (7)$$

and

$$0 \leq a_i \leq 1. \quad (8)$$

The likelihood function is defined as the product of probabilities of all stars in the CMD:

$$L = \prod_{j=1}^{n_j} p_j = \prod_{j=1}^{n_j} \left[ \sum_{i=1}^{n_i} a_i p_{ij} \right] \quad (9)$$

$$\ln(L) = \sum_{j=1}^{n_j} \ln \left( \sum_{i=1}^{n_i} a_i p_{ij} \right). \quad (10)$$

One can then use a maximisation technique to determine the weights of each isochrone, and hence the star formation and metal enrichment histories. Our method maximises the log-likelihood using a genetic algorithm to find

<sup>1</sup> Helium content also affects stellar properties but all authors assume that  $Y$  (helium content) scales linearly with metallicity  $Z$ . In this paper we use  $\Delta Y / \Delta Z = 1.4$  from Pietrinferni et al. (2004). We also use the observable  $[\text{Fe}/\text{H}]$  rather than  $Z$  for the metal abundance; see Pietrinferni et al. (2004) for the conversion.

the combination of weights  $a = (a_1, a_2, \dots, a_{n_i})$ , that most likely produced the observed CMD.

In order to interpret this as a star formation history, the weights for each isochrone need to be rescaled to account for those stars that are not in the CMD due to incompleteness effects, and those stars that have evolved beyond the final stage covered by the isochrones (either the end of the asymptotic giant branch phase or central carbon ignition, depending on the age). For instance, if a “galaxy” has had two bursts of star formation of same intensity (i.e. same total mass formed in each), one 12 Gyr ago and the other 100 Myr ago, there will be many more stars in the CMD from the young component. All stars with  $M \gtrsim 0.8M_\odot$  from the old component will have disappeared (they have evolved beyond the end of the asymptotic giant branch) and the young burst will appear much stronger than the old one. The number of missing stars in the CMD for each isochrone can be estimated from the IMF and completeness functions and added to its weight. The weights are then renormalised to give the correct relative number of stars formed at each age and metallicity.

## 2.2 Genetic Algorithm

The maximum likelihood solution is found using a genetic algorithm. This is a global optimization technique, inspired by the concept of evolution. Here we will just give a brief outline of the general procedure. To begin with, a population of randomly generated potential solutions are created and the fitness of each member is evaluated. Each individual solution is composed of a sequence of parameters/genes, which is referred to as its genotype. Members from the current generation are selected, with a probability proportional with their fitness ranking, to ‘breed’ and produce the next generation of solutions. The breeding process involves two operations: crossover and mutation. The crossover operator randomly combines the genes of the two parents, allowing for the passage of information between generations. The mutation operator randomly replaces existing genes with new genes, allowing for large leaps in the parameter space and prevents the algorithm being trapped by local maxima. This process is iterated over many generations until the algorithm converges to the global maximum.

For this problem, the genotype of each solution is the list of weights for the isochrones that characterise the star formation history. The fitness is evaluated by the likelihood. Since the parameters are linearly constrained by equation 8, our genetic algorithm adopts the same approach as Michalewicz & Janikow (1991). The weights are represented as an array of floating point numbers and the crossover and mutation operators are modified to preserve the linear constraints between generations. We have found this approach to give a faster and more reliable convergence to the global maximum than a traditional genetic algorithm as found in Charbonneau (1995).

## 2.3 Error Analysis

Uncertainty in the star formation history will arise from stars in the population being associated with the wrong isochrone due to overlap of isochrones in the CMD, imperfect models, observational effects and uncertainty in distance

and reddening values. The fact that we are using a discrete set of isochrones to model a continuous range of age and metallicity will also contribute to the uncertainty. Thus we need to calculate confidence intervals for the weights of each isochrone.

Isochrone weights with similar age and metallicity will be very highly correlated in the solution (because they are close in the CMD). They, therefore, cannot be treated as independent parameters. For this reason we estimate the confidence intervals of all the weights simultaneously using a Monte Carlo method. In a large sample limit, the likelihood function approximates an  $n$ -dimensional Gaussian at the global maximum, where  $n$  is the number of parameters (i.e. number of isochrones). Following this, it can be assumed that a  $n$ -dimensional confidence region  $Q$  will have a chi square distribution. We can determine  $Q_\gamma$ , as the limit of confidence region, which has a coverage probability  $(1 - \gamma) = 0.683$  and thus define a lower limit to the log-likelihood using

$$\ln L_{\text{lim}} = \ln L_{\text{max}} - \frac{Q_\gamma}{2}. \quad (11)$$

The limit in log-likelihood corresponds to solutions of the SFH  $1\sigma$  from the maximum. We use a Monte Carlo approach to generate solutions with a likelihood above this limit and determine the range in weights for each isochrone.

The limit in log-likelihood  $\ln L_{\text{lim}}$  is determined by the number of free parameters. Although our SFH is initially evaluated using a full library of isochrones, covering the largest possible range of age and metallicity, typically only a subset will actually contribute to the maximum likelihood solution. We will only include isochrones that have a weight greater than 0.1% in our error analysis. Isochrone with a non-zero weight below this limit do not contribute significantly to the SFH solution and are most likely just a statistical artefact of the method. This statistical artefact is seen for data with small photometric errors, where individual stars that are associated with low-weight isochrones have more of an impact on the likelihood function. The inclusion of isochrones with weights  $\leq 0.1\%$  in the error analysis has the effect of increasing the errors on all isochrones in the solution by lowering  $\ln L_{\text{lim}}$  rather than being a genuine source of variance for the distribution of stars in themselves.

Generally speaking, the greater the photometric error, the greater the confidence limits. This is due to the fact that increasing the photometric error decreases the ability of the probability to distinguish between neighbouring isochrones. Although it is essential to evaluate the star formation history using all the isochrones to achieve the highest resolution in age and metallicity possible, the resolution may be too high, depending on the quality of the data, to effectively and accurately present the resulting star formation history. This is particularly an issue for old stars, where there is very little difference between neighbouring isochrones. One way of reducing errors in the weights and therefore uncertainty in the star formation history solution is to combine isochrones into age and metallicity bins, where the weight of each bin is the sum of the weights of the isochrones it contains. Error bars on individual weights (before binning) may be large because stars can move between neighbouring isochrones; when we bin isochrones however, stars can move inside a single bin but it’s more difficult to move outside of it.

## 2.4 Implementing the Method

In the implementation of this method we use BaSTI isochrones (Pietrinferni et al. 2004). These densely sampled isochrones each consist of 2000 mass points, with a fixed number of points for each evolutionary phase (e.g. MS, SGB, RGB, HB). It is important to note that the probability function requires an integration along the isochrone, which is estimated using a discrete set of points rather than a continuous line. This means that for CMD data with small photometric error, the sampling of the isochrones can become significant in determining the probabilities. This is an important reason why we chose this particular grid of isochrones. Poor sampling can actually result in stars not registering a significant probability for the correct isochrone because they lie midway between two points. This is particularly a problem for the Main Sequence of young isochrones where a relatively small number of mass points cover a large extent in magnitude space. Since the MS is the area of greatest overlap between isochrones with the same metallicity but different ages, insufficient sampling of points on young isochrones can bias the recovered star formation history to higher ages. We find that the magnitude spacing between adjacent points on the isochrone should be no greater than the photometric error  $\sigma$  of the star, to give a reasonable approximation of the probability. We increase the sampling of points through linear interpolation so that the spacing is less than  $\sigma/2$  when integrating over the isochrone.

The isochrone grid we use has 51 ages ranging from 30 Myrs to 13 Gyrs and 11 metallicities ranging from  $[\text{Fe}/\text{H}] = -2.27$  to  $[\text{Fe}/\text{H}] = 0.4$ . As discussed previously, our method is attempting to map a continuous distribution of possible ages and metallicities on a discrete grid of isochrones. This simplification necessitates an additional error term in our probability function, which we have denoted  $\sigma_{\text{iso}}$ . Specifically  $\sigma_{\text{iso}}$  is the minimum error required for each star in the CMD to register a non-zero probability with the correct (i.e. nearest) isochrone in the grid. Ideally  $\sigma_{\text{iso}}$  would also incorporate the uncertainty in photometric magnitudes due to errors in the models as well as that due to the quantisation in age and metallicity, however this is very difficult to quantify. For now, we take a simple estimate of  $\sigma_{\text{iso}}$  based on our isochrone grid. We use  $\sigma_{\text{B,iso}} = 0.015$ ,  $\sigma_{\text{V,iso}} = 0.03$  and  $\sigma_{\text{I,iso}} = 0.019$ , which is the average difference in magnitude of a MS star with the same age and mass but neighbouring metallicities. We only estimate these “errors” using differences in metallicity because this has a much greater effect on the magnitude of stars than age, given the isochrone grid we use. The inclusion of  $\sigma_{\text{iso}}$  is very important for datasets with small photometric error (see sec 4.1 and sec 6). It ensures that stars with small photometric uncertainty do not “fall through the cracks” in our isochrone grid and that the resulting maximum likelihood solution will be a product of all the stars in the CMD.

Another point to note about the method is that the fit will be dominated by the lowest mass stars. This is due to the IMF term in the probability function and the fact that these stars have hardly evolved at all. For sufficiently deep data these stars will reside in the area of greatest overlap between isochrones of different ages in the CMD. Therefore the lower MS will contain relatively little information distinguishing age in complex stellar populations. (The effects of

metallicity on the MS can be mimicked by reddening). We apply a magnitude cut to the isochrones and the CMD to remove the lower MS stars. We ensure that this cut is taken below the MS turnoff of the oldest stars in the population. This increases the influence of the more discriminating post MS evolutionary stages in determining the star formation history.

## 2.5 Observational effects

There are two effects that we need to consider before going further. In most real situations, crowding is sufficiently important that one needs to perform artificial star experiments. Such tests consist in “injecting” stars in CCD images at random locations, doing photometry on the images, and comparing the input magnitudes with the recovered magnitudes. While these tests are usually done to determine the completeness level of the data, they also reveal the extent of the biases that affect the magnitudes and the associated errors.

*Photometric errors:* In crowded fields, photometry is done by fitting a point-spread function to the stellar images. The uncertainties returned by a photometry program do not account for the fact that nearby stars contaminate the fit. Numerous artificial star experiments have shown that the true errors are significantly larger than what is returned by a photometry program (Aparicio & Gallart 1995; Olsen, Blum, & Rigault 2003) and, at any given magnitude, they are not necessarily Gaussian in shape. Our formulation (eq. 1) uses a Gaussian function but it does not need to be so. In a real case, we would perform artificial star tests and determine the magnitude dependence of the error law and its shape (i.e. accounting for the fact that, at a given magnitude, errors are not symmetrically distributed). Knowing this, we can modify the code to account for the known distribution of errors.

*Magnitude bias:* Artificial star tests also reveal a magnitude bias in the sense that the recovered magnitudes are brighter than the input magnitudes (Aparicio & Gallart 1995; Olsen, Blum, & Rigault 2003; Stephens et al. 2001). Furthermore, the deviation gets larger and larger when the magnitude gets fainter and fainter. In our method, we would not correct the observed magnitudes but we would change the input isochrones. Knowing the extent of the bias as a function of magnitude, we can correct the magnitudes in each isochrone, i.e. subtract the appropriate deviation as a function of magnitude.

Together, these two effects would have to be implemented differently for each particular stellar system we consider. We have not done this in this paper because we focused on the method itself and its accuracy. The exact shape of the error law (i.e. what goes in eq. 1) and the exact shapes of the isochrones are not relevant for the tests we describe in this paper.

## 3 SIMPLE STELLAR POPULATIONS

In this section and section 4, we perform tests to confirm the validity of the method for the special case of simple stellar populations. Simple stellar populations are the product of a single burst of star formation, where all the stars can be

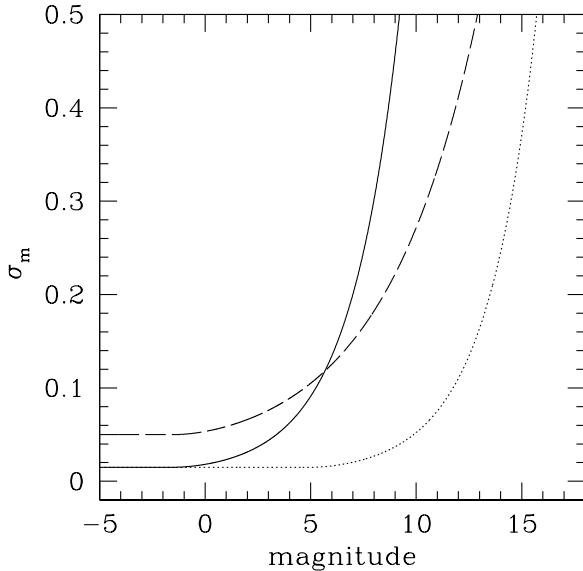


**Figure 1.** Effects of various parameters on the adopted error law. The solid line is eq. 12, the dashed line is eq. 12 but with  $\beta = 0.27$  and  $\sigma_A^0 = 0.05$ , the dotted line is eq. 12 but with  $A_0 = 5$ .

considered to have the same age and metallicity. In other words, all the stars in the population originate from a single isochrone. The problem of determining the star formation history simplifies to using the likelihood function to identify the best-fitting isochrone. This version of the method is very similar to a method used to determine the parameters of star clusters devised by Hernandez & Valls-Gabaud (2008). However, unlike these authors we are not attempting to determine these parameters precisely, but to identify the closest age, metallicity, distance and reddening from a preset grid of isochrones. For this reason and the fact that ranges of distance and reddening values can usually be constrained from the literature, it is not necessary to include optimisation from a genetic algorithm. We simply calculate the likelihood of all the possibilities in our reduced parameter space.

We test the method using both synthetic data in this section and on cluster data in section 4. The advantage of using synthetic data is that the underlying star formation history is known. Also since the CMD is created and analysed using the same models, we can properly test the strengths and weaknesses of the method without having to factor in issues with the stellar evolutionary models. We generate our synthetic CMDs using the BaSTI webtools (Cordier et al. 2007) and, unless otherwise stated, the solar-scaled no-overshooting set of isochrones. For these tests we use  $V$  and  $I$  magnitudes.

Photometric errors on magnitude  $A$  were simulated using the following typical error law:

$$\begin{aligned} \sigma_A &= \sigma_A^0 & \text{if } A \leq A_0 \\ &= \sigma_A^0 \frac{e^{\beta(A-A_0)}}{1 + \beta(A-A_0)} & \text{if } A \geq A_0 \end{aligned} \quad (12)$$

where  $\beta = 0.5$ ,  $\sigma_A^0 = 0.015$  and unless otherwise stated  $A_0 = -1.5$ . Examples of this error law are shown in Fig. 1.

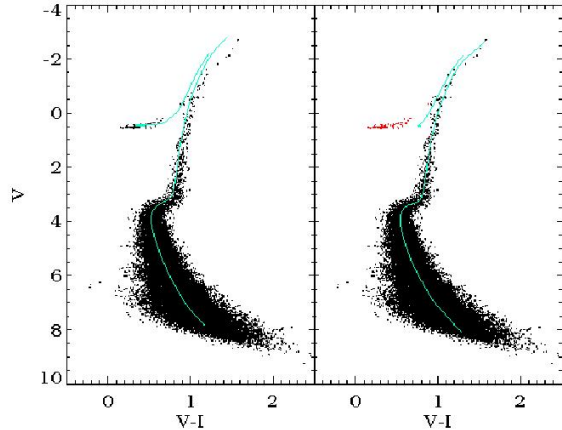


**Figure 2.** HB test: CMD of SSP (input  $t=11$  Gyr,  $[\text{Fe}/\text{H}] = -1.27$ ) with output isochrone for tests *i* and *ii* ( $t=13$  Gyr,  $[\text{Fe}/\text{H}] = -1.79$ ) on the left and tests *iii* and *iv* ( $t=11$  Gyr,  $[\text{Fe}/\text{H}] = -1.27$ ) on the right. The red points in the right panel are those stars that were removed for tests *iii* and *iv*.

**Table 1.** Results for HB tests. The input isochrone has (11 Gyr,  $-1.27$ )

test	t (Gyrs)	[Fe/H]
<i>i</i>	13	-1.79
<i>ii</i>	13	-1.79
<i>iii</i>	11	-1.27
<i>iv</i>	11	-1.27

We use synthetic simple stellar population data to test that the method can recover the correct isochrone for an old (12 Gyr,  $-1.27$ ) intermediate age (2 Gyr,  $-1.27$ ) and young (100 Myr,  $-0.25$ ) SSP. As a self-consistency check, we created a CMD for each of these SSP (with photometric errors) and verified that the method recovered the input parameters. We then perform tests to investigate how the HB, binaries, blue stragglers, the IMF and completeness in the CMD affects the results. In these cases the distance and reddening are assumed to be known and are not solved for simultaneously.

### 3.1 HB Morphology

The location of Helium burning stars in the CMD is not only dependent on the age and initial chemical composition of the population, but also on the mass loss on the RGB. As a consequence, old stellar populations of the same age can display different HB morphologies. In particular, mass loss is poorly understood and its treatment is a shortcoming of stellar models. The BaSTI isochrones use an empirically derived fixed law with a free parameter  $\eta$  either set to 0.2 or 0.4 (Pietrinferni et al. 2004) to simulate mass loss. To test the robustness of the method against data with a different HB morphology, we create a CMD with  $\eta = 0.4$  and solve for isochrones with  $\eta = 0.2$ . In this case the isochrones are underestimating the amount of mass loss occurring on the RGB and subsequently the HB phase on the isochrone is redder than the CMD data. For this test, the synthetic SSP was generated with an age of 11 Gyrs and metallicity

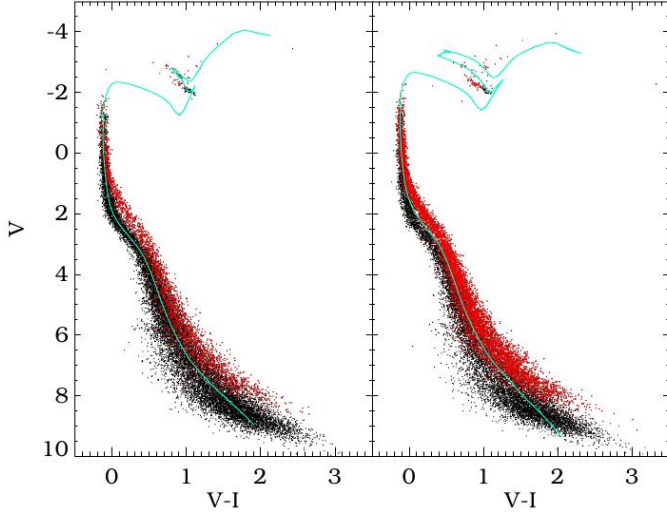


**Figure 3.** CMD of SSP (input:  $t=100$  Myr,  $[\text{Fe}/\text{H}] = -0.25$ ) with selected isochrones for binary fraction  $=0.2$  (output:  $t=100$  Myr,  $[\text{Fe}/\text{H}] = -0.25$ ) on the left and  $0.5$  (output:  $t=80$  Myr,  $[\text{Fe}/\text{H}] = 0.06$ ) on the right. The binary stars are indicated by red points.

$[\text{Fe}/\text{H}] = -1.27$ . We evaluate the parameters of the SSP with *i*) the full isochrones and the CMD, *ii*) the HB phase removed from the isochrones, *iii*) HB stars removed from CMD but using the full isochrones, and *iv*) removing HB phase from isochrones and HB stars from CMD. The results are presented in Table 1 and Fig. 2.

The results show that HB morphology can cause the method to select the wrong isochrone. In this case, a bluer HB leads to a lower metallicity and greater age. However it appears that the method can perform the fit successfully only using MS, SGB and RGB phases since the correct isochrone was selected when the HB stars were removed from the dataset.

### 3.2 Unresolved Binaries

In the CMD, unresolved binaries are most evident on the MS, where they form a second, brighter and redder sequence of stars. For post MS phases, the light of the giant star will completely dominate that of its MS companion. In order to test the effects of unresolved binaries we generated CMDs with different binary fractions, from 0.1 to 0.5 for our young, intermediate and old SSPs. The mass ratio follows a flat probability distribution between 0.7 and 1. The results for 0.2 and 0.5 are summarised in Table 2.

The method appears to be relatively robust against binaries for the intermediate and old SSPs, but not for the young population. For a high binary fraction, the method selects an isochrone with a higher metallicity and lower age than the input values (see Fig. 3). This is unsurprising since the post-MS evolutionary phases are not well populated for a young SSP and the results are more dependent on fitting the MS. However, if we take a relatively high MS cut (e.g. just below the MSTO), then the post evolutionary phases have more weight in the fit and the method selects the correct isochrone.

**Table 2.** Results for different unresolved binary fractions

Input			Output	
$t$ (Gyrs)	$[\text{Fe}/\text{H}]$	binary fraction	$t$ (Gyrs)	$[\text{Fe}/\text{H}]$
0.1	-0.25	0.2	0.1	-0.25
0.1	-0.25	0.5	0.08	0.06
2	-0.25	0.2	1.75	-0.25
2	-0.25	0.5	1.75	-0.25
12	-1.27	0.2	12	-1.27
12	-1.27	0.5	11.5	-1.27

### 3.3 Blue Stragglers

Blue stragglers are bright blue stars that inhabit the region just above the Main Sequence Turn Off in a CMD. There are two possible mechanisms suggested for blue straggler formation: stellar mergers by collision (Bailyn 1995) and mass transfer and coalescence in binary systems (Carney et al. 2001). In galactic globular clusters, the frequency of blue stragglers normalised to the number of HB stars varies between 0.1 and 1 (Piotto et al. 2004).

It is necessary to test the robustness with respect to the presence of blue stragglers in the data set because they lie close to the MSTO, which is the main age indicator in terms of isochrone fitting. We generate an SSP with (age,  $[\text{Fe}/\text{H}]$ ) = (12 Gyrs, -2.27) and add the maximum fraction of blue stragglers (i.e. a ratio of BS to HB stars of 1). We create our blue stragglers by taking stars from the MS of an SSP with (age,  $[\text{Fe}/\text{H}]$ ) = (5 Gyrs, -2.27) with a range in  $V$  from the MSTO magnitude to 1 magnitude above the MSTO in our original CMD. The method selected the correct isochrone, suggesting that blue stragglers are not numerous enough to affect the fit of the MSTO.

### 3.4 IMF and Completeness

The IMF and completeness both affect the distribution of stars along different evolutionary phases in the CMD. In the method the IMF is assumed to be a power law with an exponent of  $-2.35$ . To check that the method is robust against an input IMF we generate an SSP with a power law IMF and solve with exponents of  $-1.35$ ,  $-2.35$ ,  $-3.35$ . We find that the correct isochrone was selected each time, although the value of the maximum likelihood was highest for the correct IMF.

Completeness on the other hand is a function of magnitude and can be different among different isochrones. We simulate the effects of completeness in the CMD using the following function:

$$c(A) = \frac{1}{1 + \exp(A - A_c)/\Delta A)} \quad (13)$$

for values of  $A_c$  between 6 and 1 and  $\Delta A = 0.1$  and  $0.5$ . We also shift  $A_0$  in the error law to correspond to a photometric error  $\sigma_A \sim 0.3$  for the lowest magnitudes present in the CMD for a more realistic simulation of photometric completeness. Our tests show that, in the case of SSPs, the method is robust against an incorrect completeness function and that the method will recover the correct isochrone for any magnitude cut taken below the MSTO.



**Table 3.** Results for M 37

	$t$ (Myrs)	$[\text{Fe}/\text{H}]$	$\mu_0$	$E(B - V)$
$m_V = 21 - 20$	500	0.06	10.9	0.21
$m_V = 19 - 14$	500	-0.25	10.6	0.29

#### 4 CLUSTERS

We now test the method on real star clusters, to ensure that the method can recover reasonable values with real data and that we can compare our results with other methods. We have chosen 3 clusters that are varied in age and metallicity; an intermediate age open cluster, M 37; a globular cluster, M 3; and an old, metal-rich open cluster, NGC 6791. We allow the distance modulus and extinction of the population to vary, with ranges of values constrained from the literature. In this case we want the method to select the nearest isochrone, distance modulus  $\mu_0 = (m - M)_0$  and reddening  $E(B - V)$  to the actual parameters of the cluster.

##### 4.1 M 37

M 37 is a well studied intermediate age open cluster, with parameters determined by several groups summarised in Hartman et al. (2008). We use  $BV$  data<sup>2</sup> from Kalirai et al. (2001), with cluster members selected by Hartman et al. (2008). The final CMD consists of 1473 stars. We note that the photometric error for the M 37 data are very small, therefore the systematic error dominates the error we put into the likelihood function. Since the CMD for M 37 contains very few post MS stars and is very deep, we fit isochrones using different magnitude cuts from  $m_V = 21$  to  $m_V = 14$ . The completeness at  $m_V = 21$  is estimated to be 0.94 (Kalirai et al. 2001), therefore we use a simple step function at our lower  $V$  magnitude cutoff as a completeness function. We also use models that include overshooting, since these are more appropriate models for clusters with ages in the range of M 37. Our initial ranges for  $\mu_0$  and  $E(B - V)$  are based on the literature, with  $\mu_0 = \{10, 10.1, \dots, 11\}$  and  $E(B - V) = \{0.2, 0.21, \dots, 0.3\}$ .

The results for M 37 are summarised in Table 3 and plotted in Fig. 4.

Different groups have obtained slightly different values for the parameters of this cluster (Hartman et al. 2008; Kalirai et al. 2001; Sills et al. 2000). The values we recover for the cluster parameters are in broad agreement with those found in those papers. A self consistent test here is to compare the results with the values determined by Salaris et al. (2009) because they are based on the same set of isochrones but used a different method. The distance was determined empirically from MS fitting and the age came from fitting TO absolute magnitudes with BaSTI isochrones, assuming  $[\text{Fe}/\text{H}] = -0.20$  and  $E(B - V) = 0.23$  from (Kalirai et al. 2005). Our values of age, metallicity and apparent distance modulus are consistent with those of Salaris et al. (2009).

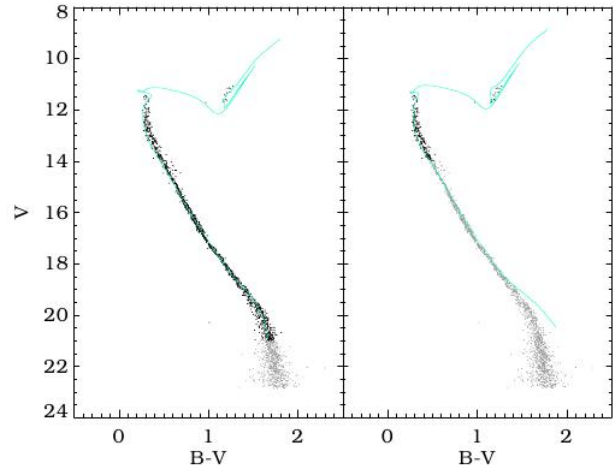


**Figure 4.** CMD of M 37 with maximum likelihood isochrone when  $m_V = 14$  (left) and  $m_V = 21$  (right), grey points indicate stars that have been removed before likelihood analysis

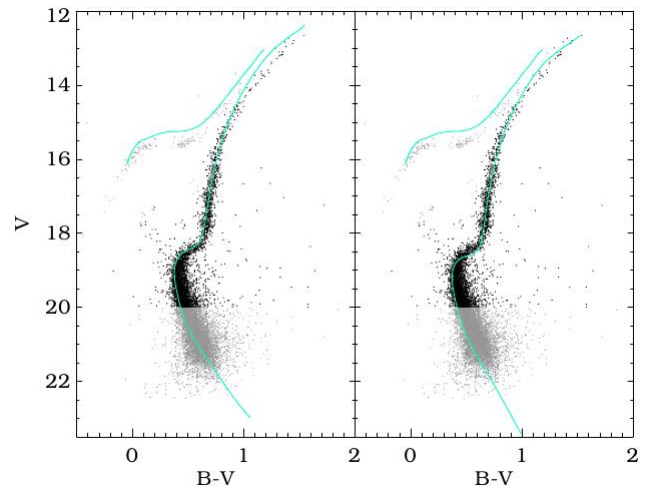


**Figure 5.** CMD of M 3 with maximum likelihood solar-scaled isochrone (left) and maximum likelihood  $\alpha$ -enhanced isochrone (right). Stars in grey have not been used in the fit.

##### 4.2 M 3

The data for M 3 are taken from Buonanno et al. (1994), with photometric errors estimated from Fig. 7 in that paper. The CMD is displayed in Fig. 5, where grey points represent stars that have been removed from the CMD prior to analysis. We have estimated the completeness function using Table 7 in Buonanno et al. (1994) and have also taken a lower MS magnitude cut at  $m_V = 20.05$ . The CMD features an extended Horizontal Branch, which has been removed and we only use points up to the tip of the RGB in the isochrones. The final CMD consists of 4173 stars.

We complete the test using both solar scaled and  $\alpha$ -enhanced isochrones. The ranges in distance modulus and extinction are  $\mu_0 = \{14.75, 14.8, \dots, 15.3\}$  and  $E(B - V) = \{0, 0.01, \dots, 0.07\}$ . The results are presented in Table 4 and Fig. 5.

Visual inspection of Fig. 5 show that the method provides a reasonable fit of isochrone to the data for both solar

<sup>2</sup> downloaded from WEBDA at [www.univie.ac.at](http://www.univie.ac.at)

**Table 4.** Results for M 3

	$t$ (Gyrs)	[Fe/H]	$\mu_0$	$E(B-V)$
ss	13.0	-1.49	15.05	0.0
ae	10.5	-1.31	15.3	0.0

**Table 5.** Results for NGC6791

	age (Gyrs)	[Fe/H]	$\mu_0$	$E(B-V)$
<i>BV</i>	8.5	0.40	13.0	0.14
<i>VI</i>	9.0	0.26	13.1	0.12
<i>BVI</i>	8.5	0.40	13.1	0.12

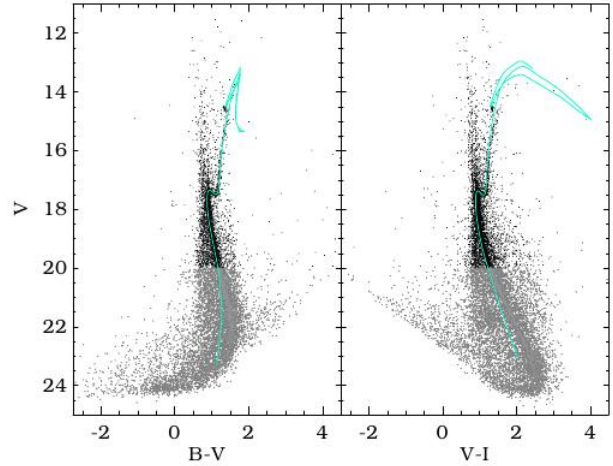
scaled and  $\alpha$ -enhanced models, although the upper RGB is not well represented by the isochrones in both cases. The solutions for the  $\alpha$ -enhanced models have a likelihood greater than the scaled solar ones, suggesting a better fit, consistent with expectation, for spectroscopy of M 3 stars shows they are  $\alpha$ -enhanced with  $[\alpha/\text{Fe}] = 0.27 \pm 0.03$  (Carney 1996).

The result from the  $\alpha$ -enhanced isochrones is consistent with literature values of the cluster parameters, e.g. the recent values found by Benedict et al. (2011), who determine  $\mu_0 = 15.17 \pm 0.12$  from an empirical calibration of the RR Lyrae distance scale (using  $E(B-V) = 0.01$  and  $[\text{Fe}/\text{H}] = -1.57$ ) and an age of 10.8 Gyr Benedict et al. (2011).

### 4.3 NGC6791

The data for NGC6791 are taken from Stetson et al. (2003). Since there are measurements in  $B$ ,  $V$  and  $I$ , we take this opportunity to determine and compare the results using different magnitude combinations. We solve for  $BV$ ,  $VI$  and  $BVI$ . There is evidently foreground contamination in the CMD for NGC6791, however we do not attempt to remove this in order to test whether the method is robust against contaminating stars. We take a magnitude cut at  $m_V = 20$ , the resulting input CMDs consist of 12763 stars. The ranges in distance modulus and extinction are  $\mu_0 = \{12.5, 12.6, \dots, 13.5\}$  and  $E(B-V) = \{0.1, 0.12, \dots, 0.2\}$ .

The results for NGC6791 are plotted in Fig. 6 and summarised in Table 5. From Fig. 6 the method appears to have provided a reasonable fit to the data despite the presence of foreground stars in the CMD. The likelihood for  $BV$  is higher than for  $VI$ , which is indicative of a better fit to the data. The  $BVI$  results fit the same age and metallicity as the  $BV$  results, but have a distance and reddening consistent with the  $VI$  results. It should be noted that  $[\text{Fe}/\text{H}] = +0.4$  is the highest in the isochrone library, so it is possible that a higher metallicity is more consistent with the data. The best set of empirical parameters (determined from eclipsing binaries) is from (Brogaard et al. 2011) who found  $[\text{Fe}/\text{H}] = +0.29 \pm 0.03$  (random)  $\pm 0.07$  (systematic),  $E(B-V) = 0.160 \pm 0.025$  and  $\mu_V = 13.51 \pm 0.06$ . Our results are in good agreement with these. Our results (particularly age) are also consistent with Bedin et al. (2011) who fit the BaSTI isochrones to HST data; they obtained  $[\text{Fe}/\text{H}] = 0.4$  and find  $E(B-V) = 0.17$ ,  $\mu_V = 13.50$  and  $t = 8$  Gyr.

**Figure 6.** CMD of NGC6791 and maximum likelihood isochrone for  $V$ ,  $B-V$  (left) and  $V$ ,  $V-I$  (right)

## 5 COMPLEX STELLAR POPULATIONS

Analysing the CMD of a complex stellar population (CSP) poses more of a challenge than SSPs, since the method not only has to be able to identify the correct isochrones in the solution but also allocate the correct number of stars to these isochrones. The synthetic SSP tests allowed us to investigate the robustness of the method in selecting the correct isochrone. For the synthetic CSP tests we complete similar tests, but now the emphasis is on whether the method can accurately reproduce different types of star formation histories. In particular we want to ascertain how well the method can distinguish between bursting and continuous star formation scenarios.

We present two star formation histories, depicted in Fig. 7, which will be referred here on in as population 1 and 2. Population 1 represents an old stellar population with constant star formation rate with ages between 3.5 Gyrs and 13 Gyrs and metallicities between  $[\text{Fe}/\text{H}] = -2.27$  and  $[\text{Fe}/\text{H}] = -0.96$ . Population 2, on the other hand, consists of two equal bursts of star formation, one with an age of 2 Gyrs at  $[\text{Fe}/\text{H}] = -0.35$  and the second with an age of 500 Myrs and  $[\text{Fe}/\text{H}] = 0.26$ .

For both populations 1 and 2 we create a synthetic CMD using BaSTI synthetic CMD generator Cordier et al. (2007). Simulated photometric errors are applied to this original CMD using the same error law as the SSP tests, but with a range of values for  $A_0$ , to test the method with different quality of photometric data. At this point, we do not include distance or reddening, but fix  $\mu_0 = 0$  and  $E(B-V) = 0$ . We solve for  $V$  and  $I$ , and take a lower MS magnitude cut at  $M_V = 6$ , which is about 2 magnitudes below the oldest possible turn-off. Note that the completeness will be 1 for all magnitudes. We test the effect of photometric incompleteness in sec 5.3.

The input CMD and recovered star formation histories for  $A_0 = 5$  are displayed in fig. 8 and 10 for population 1 and 2 respectively.

The method was able to reproduce the overall star formation history for several values of  $A_0$  in the error law. However the weights of the isochrones fluctuate more from their true values with data that has a greater photometric



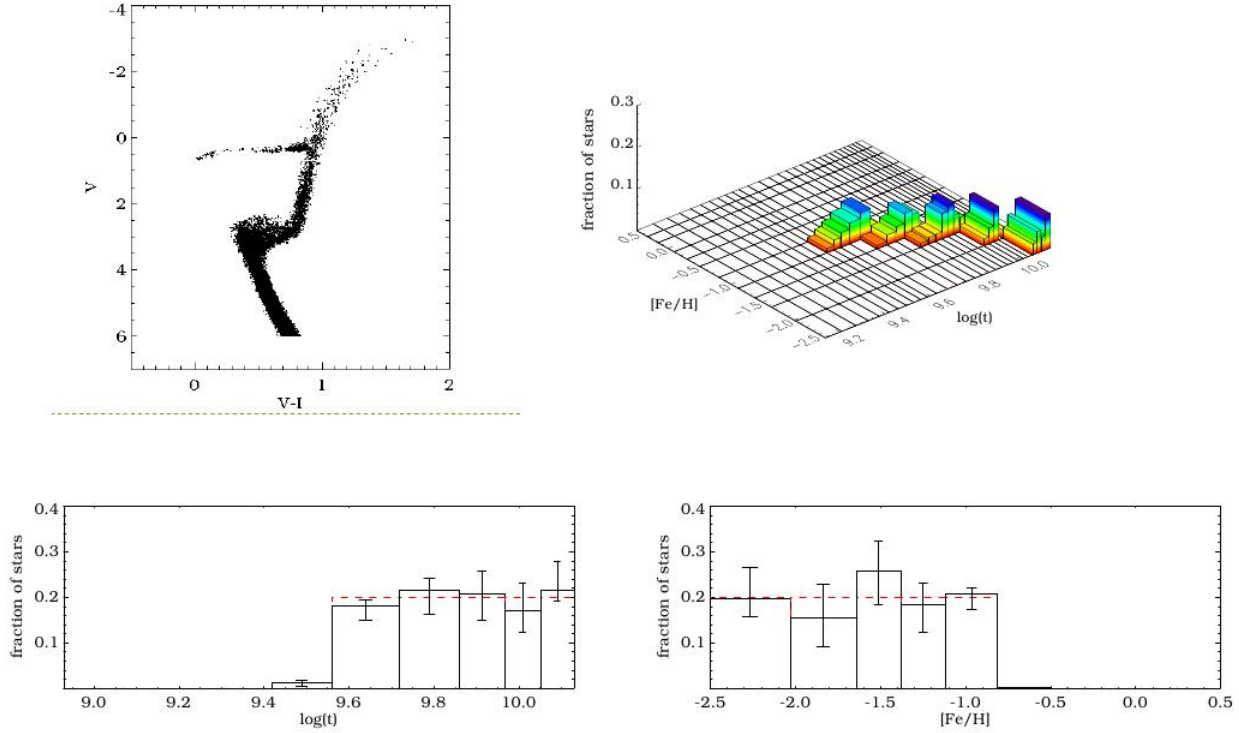


**Figure 8.** Results for pop. 1 ( $A_0 = 5$ ): *Top left*: input CMD *top right*: plot of the full recovered star formation history, *bottom left*: plot of the relative star formation rate as a function of time *bottom right*: plot of the relative star formation rate as a function of metallicity. The input SFH solution is plotted in red for comparison in the bottom two panels.

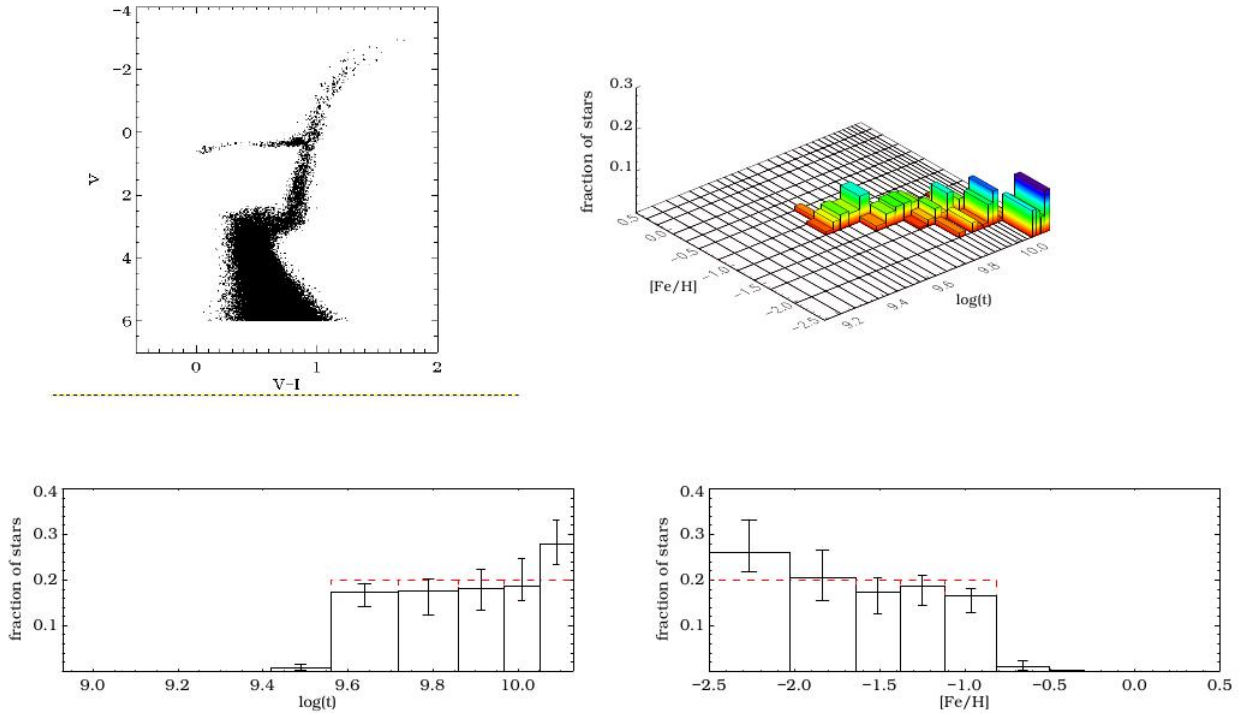


**Figure 9.** Results for pop. 1 with  $A_0 = -1.5$  (same format as in Fig. 8)

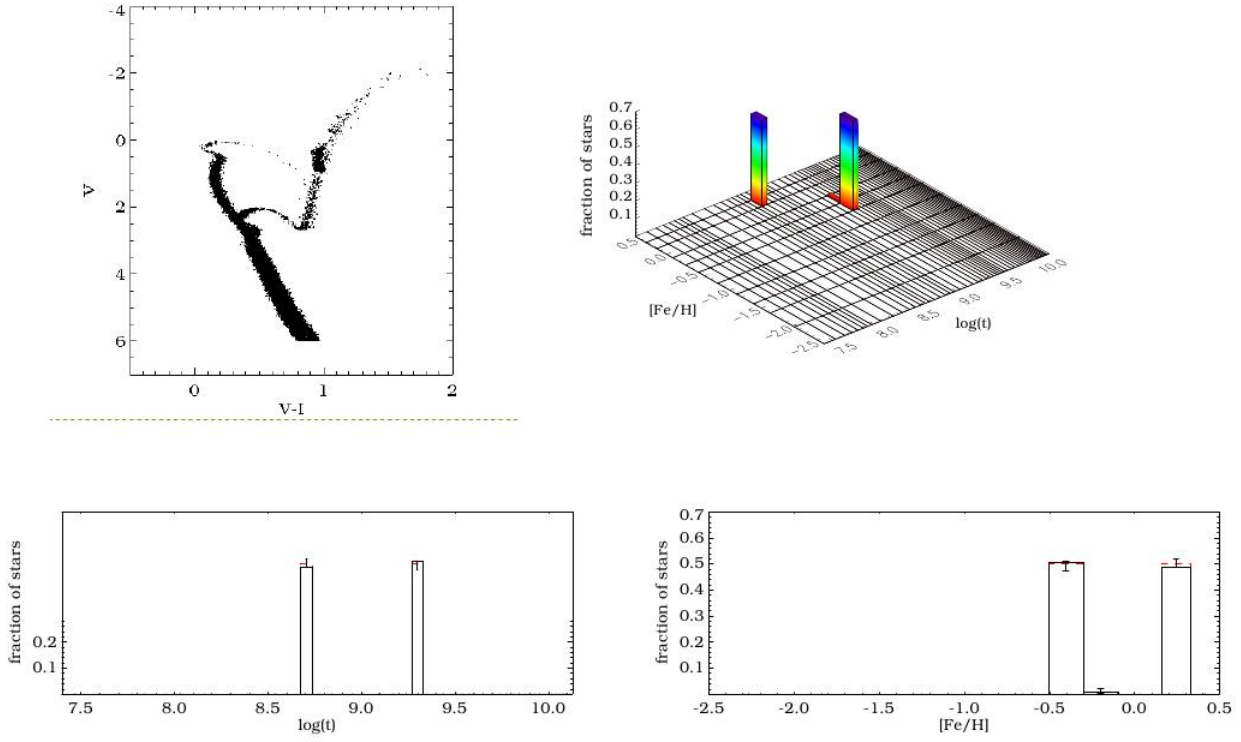


**Figure 10.** Results for pop. 2 (same format as in Fig. 8)

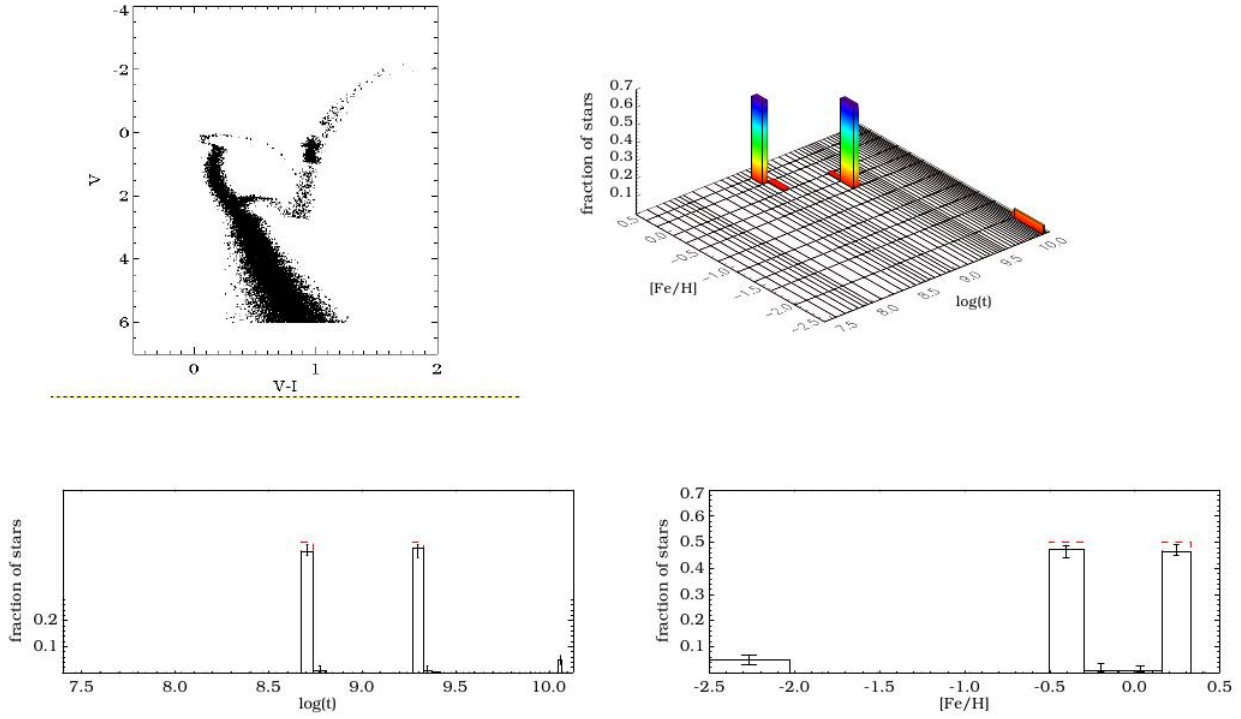


**Figure 11.** Results for pop. 2 with  $A_0 = -1.5$  (same format as in Fig. 8)

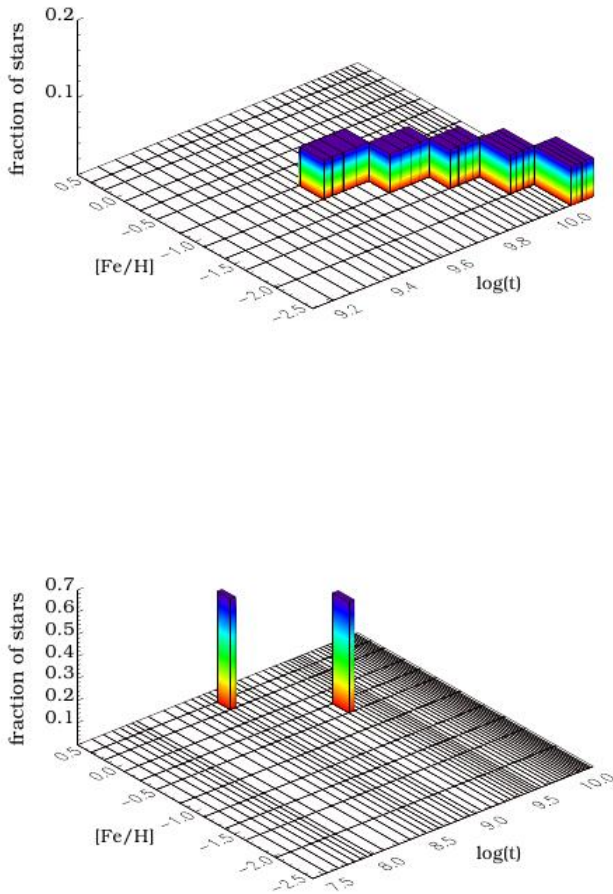


**Figure 7.** Input star formation histories for population 1 (top) and population 2 (bottom). The x and y axes represent age and  $[\text{Fe}/\text{H}]$ , each rectangle representing an isochrone. The vertical axis represents the fraction of stars at each age and metallicity, which is essentially the weight of each isochrone.

error. This is understandable since the isochrones that are close in age and metallicity are also close in the CMD, and large photometric errors diminish the distinction between these isochrones in terms of their relative probability. Our tests for population 1 show that when the photometric errors increase (at a given magnitude) this causes oscillations or even gaps in the star formation rate due to stars, originating from one isochrone, being accounted for entirely by neighbouring isochrones. This could be misinterpreted as a varying or bursting star formation rate, so it is always important to calculate confidence limits and present the results using suitable age and metallicity bins.

We also test the effect of increasing and decreasing the photometric errors of stars in the synthetic CMD by factors of 2 and 5 to mimic the effect of estimating errors inaccurately. Overestimating errors has the effect of increasing the “burstiness” of the star formation history solution.

For population 1, although each input metallicity is represented in the solution, stars become more concentrated on the central age of each subpopulation. Also more stars are given to the subpopulation with the mid-range metallicity. For population 2, the bursty star formation is actually recovered better with the overestimated errors than with the original errors. On the other hand, underestimating errors

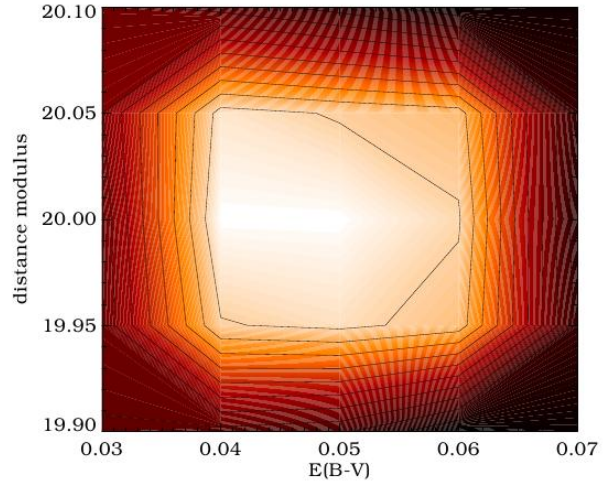


**Figure 12.** Contour plot of likelihood for pop. 1 with input  $\mu_0 = 20$ ,  $E(B - V) = 0.05$  against distance and reddening

increases the apparent duration of the star formation events and adds spurious isochrones into the solution.

We also generate a CMD for population 1 with a distance modulus  $\mu_0 = 20$  and  $E(B - V) = 0.05$ , to test whether we can use the method to estimate these parameters as well as determine the star formation history. We simulate the photometric error using eq. 12 with  $A_0 = 18.5$ . We determine the maximum likelihood star formation history for distances  $\mu_0 = \{19.9, 19.95, \dots, 20.1\}$  and reddenings  $E(B - V) = \{0.03, 0.04, \dots, 0.07\}$ . The maximum likelihood solution recovers the input values of reddening and distance modulus *as well as* the same SFH as in the previous case. Fig. 12 shows how maximum likelihood changes with distance and reddening values.

### 5.1 Unresolved Binaries

The SSP tests showed that the method was sensitive to the effects of binaries only for a high binary fraction and for young stellar populations. As we are no longer forcing the method to select a single isochrone, but to attribute stars to a combination of isochrones, it is expected that unresolved binaries will have a different effect on the recovered star formation history. To perform this test, we generate synthetic CMDs for population 1 and 2 with a binary fraction of 0.4 and the same mass ratio distribution as the SSP tests. We perform the test using two error laws:  $A_0 = 5$  and  $A_0 = -1.5$ . We also apply a distance modulus  $\mu_0 = 20$  and reddening  $E(B - V) = 0.05$  to the synthetic data and simultaneously test how binaries affect these recovered parameters. The range of values are  $\mu_0 = \{19.75, 19.8, \dots, 20.05\}$  and  $E(B - V) = \{0.04, 0.05, \dots, 0.09\}$ .

The CMD and recovered star formation history for population 1 with  $A_0 = 25$  is displayed in Fig. 13. It is evident from the CMD that the population of binary stars (red points) on the MS are distinct from the single stars (black points). For the  $A_0 = 18.5$  case, the photometric error effectively mixes the two together on the MS. For the correct value for  $\mu_0$  and  $E(B - V)$ , the binaries are seen in the maximum likelihood solution as an additional population of

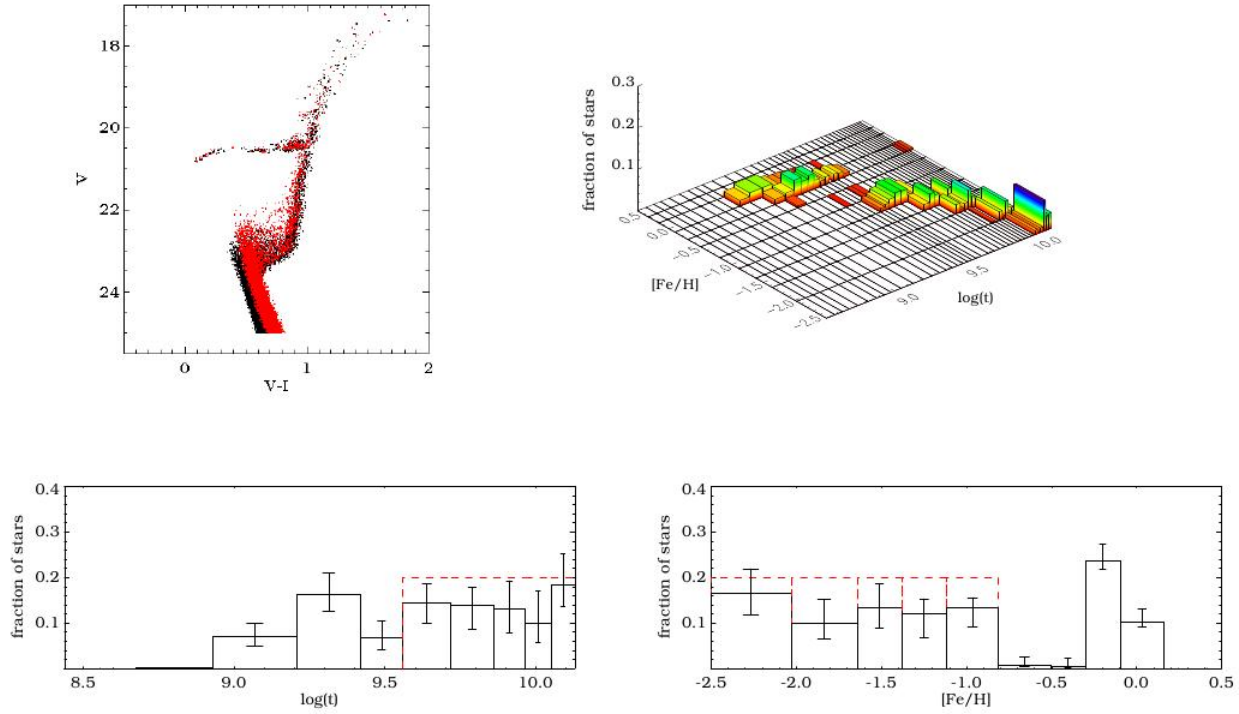


**Figure 13.** CMD and recovered star formation history for pop. 1 with binary fraction = 0.4 (same format as Fig. 8). The red stars in the CMD are the binaries.

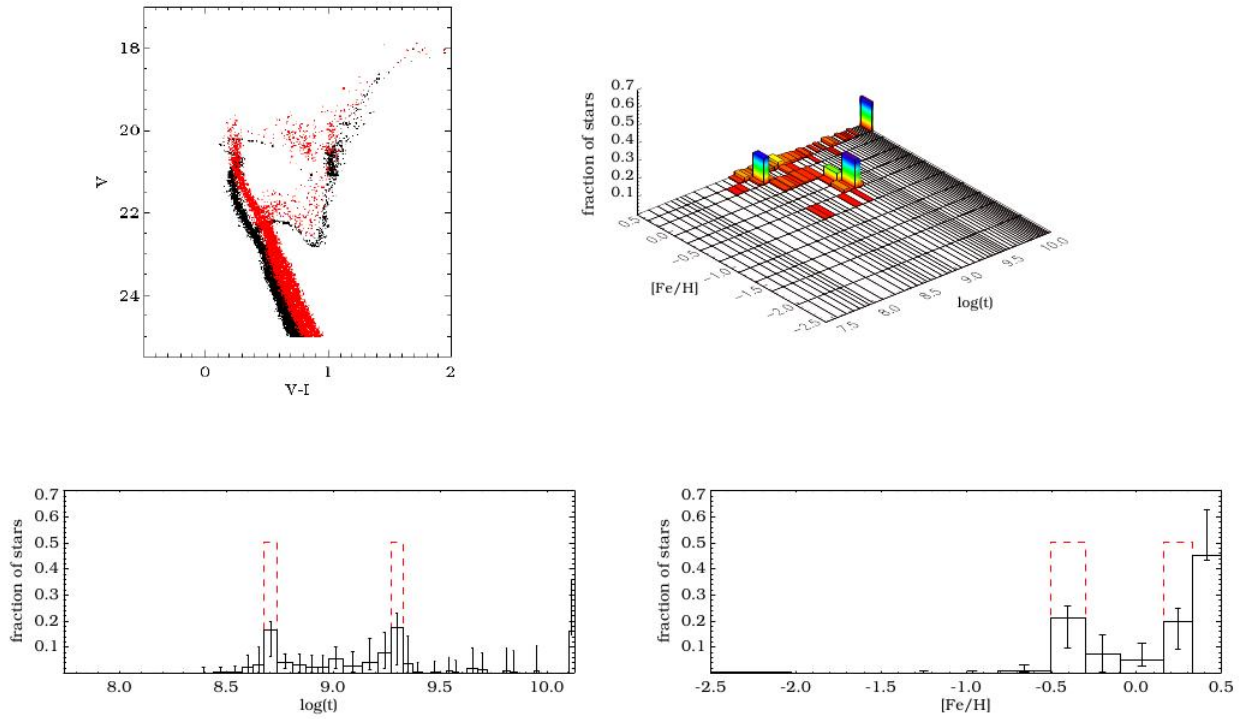


**Figure 14.** CMD and recovered star formation history for pop. 2 with binary fraction = 0.4 (same format as Fig. 8). The red stars in the CMD are the binaries.

younger and more metal rich stars. In Fig. 13, the binaries are evidently separate from the rest of the solution, whereas for  $A_0 = 18.5$  the binaries are seen as an extension of the main star formation epoch. Nevertheless, the rest of the star formation history is recovered quite well in both cases. The method estimated the distance and reddening correctly for  $A_0 = 25$ , but there was a small shift to a lower distance modulus  $\mu_0 = 19.95$  for  $A_0 = 18.5$ . This could possibly be attributed to binaries close to the MSTO. The shift in  $\mu_0$  is too small to have a significant effect on the recovered star formation history.

For population 2 we encounter the same problem as we did for the young SSP case. The fit is dominated by the MS, and the effects of binaries on the recovered star formation history are more dramatic. Unfortunately we cannot deal with binaries in the way we did for SSP since we can only take a magnitude cut below the TO of the oldest stars in the CMD without losing age information provided by the TO and SGB. This still leaves a significant amount of MS binaries in the data.

The CMD and recovered star formation history of population 2 for  $A_0 = 18.5$  is presented in Fig. 14. For the younger burst, the MS and binary sequence are very distinctly separated in the CMD for both error laws. If  $\mu_0$  and  $E(B - V)$  are fixed to the correct values, the centres of two bursts are recovered correctly in the maximum likelihood solution. However stars are also attributed to other isochrones, particularly those with the highest metallicity. The age spread at this metallicity may be due to the fact that the younger burst is close to the edge of our ischrone grid, so that binaries too red to be attributed to a single MS are being fit by MSTO and subgiant branch of older isochrones instead.

If the distance modulus and reddening are left as free parameters then the maximum likelihood solution is at  $\mu_0 = 20$  and  $E(B - V) = 0.05$  for  $A_0 = 25$  and  $\mu_0 = 19.75$  and  $E(B - V) = 0.07$  for  $A_0 = 18.5$ . We note that  $\mu_0 = 19.75$  is the lowest in our range and the actual maximum solution may be at an even lower distance. If this is the case then it suggests that distance and reddening parameters are not being constrained at all by the post-MS stars. The derived star formation history is also affected by the incorrectly estimated parameters. The centres of the two bursts are shifted to a lower metallicity  $[\text{Fe}/\text{H}] = 0.06$  and  $[\text{Fe}/\text{H}] = -0.66$  to compensate for the higher reddening. The age of the younger burst is also lower, although the age of the older burst remains the same. The reason that distance and reddening results are only affected in the  $A_0 = 18.5$  case is that the photometric error effectively blurs the distinction between single and binary stars and gives greater leeway in fitting the isochrones. The parameters are skewed as the method attempts to find an average fit for both populations. On the other hand, single and binary stars remain distinct when the photometric errors are small and the overall distance and reddening parameters of the whole population are dominated by the more numerous single stars.

To summarise, binaries do affect the recovered star formation history by taking stars away from correct isochrones and populating younger, more metal rich isochrones. Binaries also transform the likelihood landscape for distance and reddening, causing it to become more complex and multi-peaked compared to Fig. 12. We have completed the tests using a relatively high binary fraction and expect similar

but less significant effects for smaller binary fractions. The effects of unresolved binaries cannot be ignored when using the method and must be a caveat in interpreting the star formation history of a stellar population with an unknown binary fraction. We will leave the subject of dealing with unresolved binaries in a fully consistent way as the subject of a future paper.

## 5.2 HB Morphology

Similar to our SSP test, we explore the effect of an incorrect HB morphology, by creating a CMD using  $\eta = 0.4$  isochrones and solved using  $\eta = 0.2$ . In the SSP tests we found that a bluer HB could lead to a more metal poor and subsequently older ischrone being selected. The point of repeating these tests for complex stellar populations is to ascertain the effect of blue HB stars when we remove the constraint that all stars of a population belong to one ischrone. We need to establish how important HB stars are in determining the star formation history. We also want to check whether blue HB stars can possibly be mistaken for young MS stars, since there can be an overlap of isochrones in the CMD.

Again we complete the tests for population 1 using the two cases of simulated photometric errors,  $A_0 = 5$  and  $A_0 = -1.5$ . We actually take a magnitude cut of  $V = 4$  rather than  $V = 6$  to increase the weight of the HB in star counts in the CMD. We evaluate the star formation history with and without the inclusion of the HB stars. There is no apparent difference between the two results for  $A_0 = 5$ , leading us to the conclusion that the HB is effectively ignored in this instance. For  $A_0 = -1.5$  we find that the star formation history is recovered slightly better when the HB is removed. The actual effect is a slight metallicity spread at some of the ages and is relatively small compared to fluctuations due to photometric error. For neither case do we falsely detect young stars due to overlap of HB stars with young isochrones.

These tests reveal that the star formation can be determined reliably without fitting HB stars. They also show that a different HB morphology can only bias the results if there is greater leeway in the fit to the MS by photometric error. This is further confirmation that the method is very much dominated by the lower mass stars in the CMD.

## 5.3 IMF and Completeness

Our SSP tests showed that the IMF and completeness do not affect the selection of the correct isochrones. However, since IMF and completeness determine the distribution of stars along each ischrone in the CMD, it is important to check that these factors do not significantly affect the ischrone weights in the maximum likelihood solution. Especially since we need to correct for our assumed IMF and completeness to get the relative number of stars formed at each age and metallicity.

For the IMF test, we populate isochrones in a synthetic CMD of our population 2 using an IMF with a power law exponent  $-2.35$ . In these tests, we simulate photometric errors using  $A_0 = 5$  so as to minimise the fluctuations in the weights caused by the photometric errors. The star formation history is then evaluated assuming exponents of  $-1.35$ ,



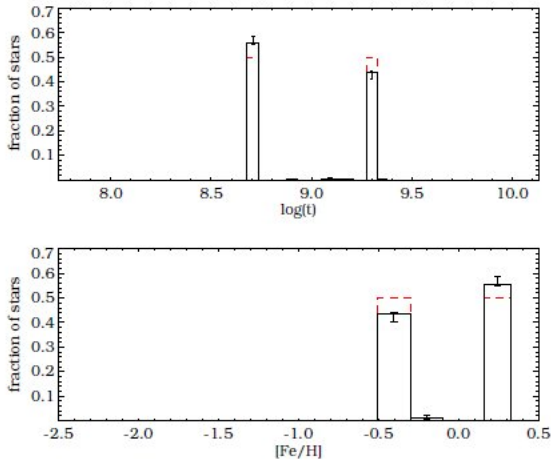


**Figure 15.** Plot of the relative star formation as a function of time and metallicity for pop. 2 with simulated incompleteness (see text for details).

−2.35 and −3.35. We note that changing the slope of the IMF power law will alter the relative probabilities of the individual stars. Increasing the exponent effectively increases the probabilities of lower mass stars compared to higher mass stars, thereby increasing their contribution to the likelihood function, and vice versa. However, our tests show that the unscaled weights for each isochrone are not affected by different IMF exponents, although the maximum likelihood is greatest for the correct value. We infer that the method is robust against an incorrect IMF.

Rescaling with an incorrect IMF will affect the final isochrone weights. We will underestimate (respectively overestimate) the number of stars needed to correct for the older burst if the IMF slope is too steep (resp. too shallow). Although this effect will vary depending on the specifics of the star formation history solution, we find that for our synthetic test the change in the weights are of the order of 5 – 10%.

We now introduce the effect of incompleteness, using equation 13 with  $A_c = 5$  and  $\Delta A = 0.45$  to remove stars from our previous CMDs for population 2. Again we simulate the errors only using  $A_0 = 5$ . The results show that the weight of the older burst is underestimated and the younger burst is overestimated by  $\sim 5$ –10% (see Fig. 15). At a given magnitude (below the TO of the oldest population) the more metal-poor MS is populated by lower mass stars than the metal-rich component. Due to the shape of the IMF, we are therefore missing more metal-poor stars than metal-rich stars. If completeness is accounted for then rescaling to a given mass range will correct for this imbalance. One way of avoiding the problem of incompleteness is to take a cut on the MS, above which one can be sure that the data will be complete or at least has no magnitude dependence due to measurement limitations.

## 6 CARINA DWARF GALAXY

The final test is to apply the method to a CMD of a real complex stellar population, the Carina dwarf galaxy. There have been many studies of its stellar populations in the lit-

erature, both spectroscopic and photometric, with which we can compare our results and there is general agreement regarding its star formation history. Our aim here is not to perform a detailed analysis of the Carina CMD to recover the SFH but to test whether we can recover what is fairly well known about this galaxy.

Studies of the SFH of Carina have identified several episodes of star formation: an initial burst at  $\sim 12$  Gyr followed by an intermediate-age event at  $\sim 6$  Gyrs, with a possible more recent episode at  $\sim 2$  Gyr (Smecker-Hane et al. 1996; Hurley-Keller et al. 1998; Rizzi et al. 2003). The intermediate age episode however can have a different duration according to different authors and this may affect the existence of the most recent one (as it “merges” with the intermediate age population). Studies based on HST data have found a more continuous SFH with one or more “peaks” (Mighell 1997; Hernandez et al. 2000; Dolphin 2002) but they do not detect a significant old population (because of the small number of stars in the field). Overall it is clear however that there was an ancient episode of star formation followed by one and possibly two others.

Because of its proximity, it is also possible to obtain spectroscopy of red giant stars in Carina to study its metal enrichment history. The consensus is that Carina is a fairly metal-poor system with an average  $[\text{Fe}/\text{H}]$  around −1.6 (Koch et al. 2006, 2008; Tolstoy et al. 2003; Lemasle et al. 2012). There may be a range in metallicity of order 0.5 dex (Tolstoy et al. 2003; Lemasle et al. 2012) or even higher depending on the method used (Koch et al. 2006). Photometric studies tend to agree on the fact that the metallicity range has to be fairly small Smecker-Hane et al. (1996); Rizzi et al. (2003); Bono et al. (2010) in order to reproduce the thinness of the RGB. More recently, Fabrizio et al. (2012) measure a more modest spread and a more metal poor mean  $[\text{Fe}/\text{H}]$  from spectroscopy of red giant stars, which is in better agreement with photometric studies.

We use the data set of Bono et al. (2010) which covers a fairly wide field and reaches well below the MS turn off of the oldest population. The CMD is already background subtracted with an algorithm described in that paper. The  $V$ ,  $B-V$  CMD is shown in Fig. 16, where black points are included and grey points have been removed from the dataset prior to analysis. Carina exhibits an extended blue HB as well as a red clump but, to avoid problems with uncertain predictions of HB morphology, we are neglecting the helium-burning phase in our analysis. We have also taken a lower MS magnitude cut at  $m_V = 24$ . We have not determined the completeness

The estimated photometric errors for this dataset of Carina are small enough that the total error is dominated by  $\sigma_{\text{iso}}$ . We solve for distance modulus and reddening simultaneously with initial values of  $\mu_0 = \{19.9, 19.95, \dots, 20.2\}$  and  $E(B-V) = \{0.03, 0.04, \dots, 0.08\}$ . We have used the solar-scaled isochrones since spectroscopic studies have shown evidence of very little  $\alpha$ -enhancement in the majority of Carina’s giant stars and other dwarf spheroidal galaxies (e.g. Shetrone et al. 2003). We have solved for  $BV$ ,  $VI$  and  $BVI$ , however we present the  $BV$  results since our likelihood calculations indicate a better fit to the data than  $VI$  or  $BVI$ . We have attempted to solve for the star formation history while leaving distance modulus and reddening as free



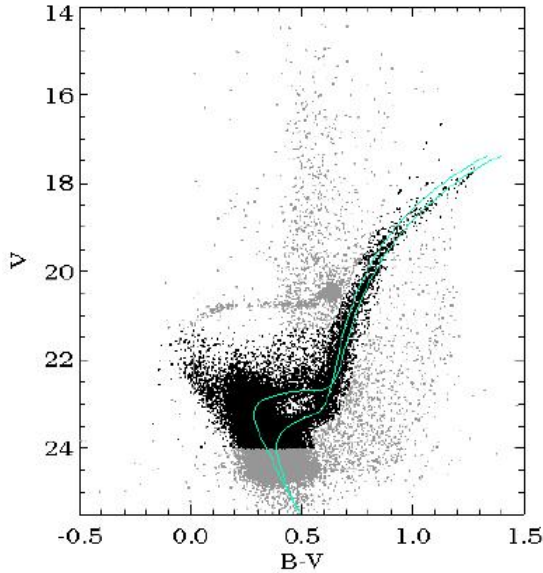


**Figure 16.** CMD for the Bono et al. (2010) dataset. The grey points represent stars removed from the dataset prior to the SFH determination

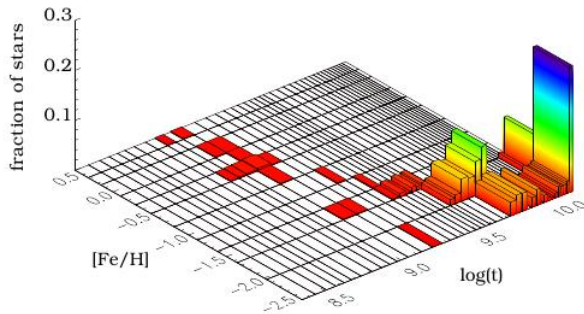


**Figure 17.** The star formation history of Carina using  $B$ ,  $V$  (isochrone weights have been rescaled). The cluster of metal-rich isochrones near 2 Gyrs is likely due to binary stars (see text for details).

parameters. For  $BV$  our maximum likelihood solution is at  $\mu_0 = 20$  and  $E(B - V) = 0.06$ .

We present the star formation history in full in Fig. 17 and as a relative star formation rate as a function of age and metallicity in Figs. 18 and 19. Our star formation history is dominated by two bursts; one centred on (13 Gyrs, -2.27) and one centred on (6 Gyrs, -1.79). We overplot the central isochrones representing each burst on the CMD of Carina in Fig. 16. Here we are using the term burst loosely to describe enhanced periods of star formation, lasting several Gyrs, interspersed with a period of negligible star formation.

Our results qualitatively agree with those of Smecker-Hane et al. (1996) and Hurley-Keller et al. (1998) and most closely resembles that of Rizzi et al. (2003). We find that the second burst formed most of its stars at  $\sim 6$  Gyrs but there is an extended tail of star formation until  $\sim 3$  Gyrs.

According to our results, 34% of stars in the CMD were formed at 13 Gyrs while 46% were formed between 4.5 and 7 Gyrs. Our solution also contains a small number of more

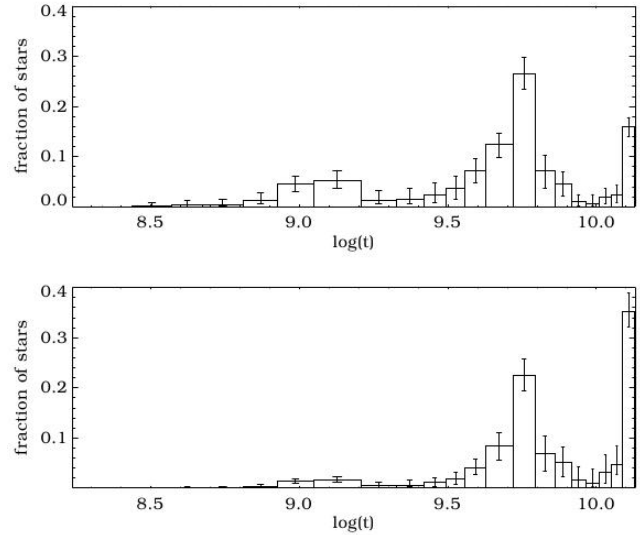


**Figure 18.** The star formation rate as a function of age for Carina based on our  $BV$  results. The top plot shows the maximum likelihood solution. The bottom plot shows the same but after having rescaled the isochrones to determine the relative number of stars formed at each age.

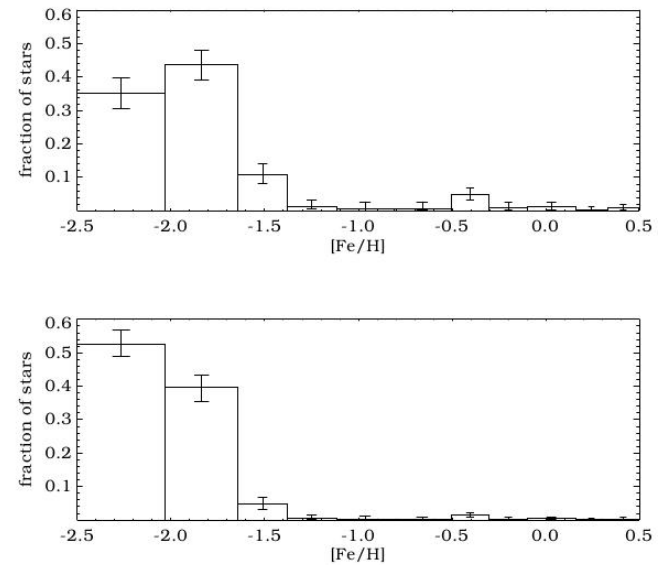


**Figure 19.** Metallicity distribution for Carina based on our  $BV$  results. The top plot shows the maximum likelihood solution. The bottom plot shows the same but after having rescaled the isochrones.

metal rich lower mass stars, around 1 Gyrs. However if we overplot the isochrone (1 Gyr,  $-0.35$ ) it is evident that there are no RGB or He burning stars belonging to this population evident in the CMD. We suspect that these are actually unresolved binaries from the more metal poor star formation events rather than a genuine metal rich sub population. If this is the case then the number of stars associated with our intermediate burst are slightly underestimated.

One of the benefits of our method is that the chemical enrichment history does not have to be assumed but can be determined self-consistently with the star formation rate.

The results indicate that Carina consists of mainly metal poor stars, with an overall mean metallicity lying between  $[\text{Fe}/\text{H}] = -2.27$  and  $[\text{Fe}/\text{H}] = -1.79$ , although weighted towards the latter. This is consistent with several studies cited above. It is lower but still compatible with Bono et al. (2010), who measure a metallicity of  $[\text{Fe}/\text{H}] \simeq -1.70 \pm 0.19$  dex, from the difference in colour between the red clump and the middle of the RR Lyrae instability strip.

Although in our results both populations have stars at both metallicities, more old stars are at  $[\text{Fe}/\text{H}] = -2.27$  and more intermediate age stars are at  $[\text{Fe}/\text{H}] = -1.79$ , in agreement with Lemasle et al. (2012). This indicates that some chemical enrichment occurred between the two bursts, although it is hard to quantify with the metallicity resolution of the isochrone grid. Our results also show a spread in metallicity within each burst; the intermediate age burst in particular has stars associated with  $[\text{Fe}/\text{H}] \sim -2.27$  to  $[\text{Fe}/\text{H}] \sim -1.49$ . Although, again we have to bear in mind our metallicity resolution, which could make this spread appear larger than it actually is. Our recovered star formation history shows an age metallicity dependence during the second period of star formation in that more metal rich isochrones are also younger. Also, since our result is also constrained by the MS and SGB, the age metallicity dependence seen is not just due to age metallicity degeneracy on the RGB.

## 7 SUMMARY AND CONCLUSIONS

We have presented a method to determine the star formation history (including its metallicity history) of any stellar population. We model the star formation history as a linear combination of simple stellar populations and determine the relative number of stars belonging to each sub population using a maximum likelihood method. Our likelihood function is constructed from the combined probabilities of all the stars in the CMD originating from the isochrones in our grid, fully taking into account individual measurement errors, IMF and completeness. The maximum likelihood is determined using all evolutionary phases in the CMD, although the fit is naturally weighted towards fitting the lower mass stars. However there is the option of removing problematic features from the CMD, such as the lower MS and HB; the star formation history is recovered reliably without these stars. The method can be used with fixed or free distance and reddening parameters. Distance and reddening can be solved for simultaneously by determining the star formation history of each combination of parameters and taking the highest of the maximum likelihoods. If the method is being used to estimate distance and reddening, it is recommended to check that the isochrones in the solution are consistent with the data when overplotted on the CMD.

The method has several advantages: *i*) it does not rely on any assumption regarding the star formation history or age-metallicity relation (Hernandez et al. 1999), *ii*) it does not require the calculation of elemental CMDs (Aparicio & Hidalgo 2009; Harris & Zaritsky 2001; Dolphin 2002; de Boer et al. 2012) but compares the data directly to the isochrones, *iii*) it does not parameterise the CMD by binning, but treats each star individually. This last point means that the method has the potential to recover very detailed

star formation histories, since no information is being lost through the binning process. The maximum possible resolution in time and metallicity of the solution will depend on the isochrone grid, however, in practice it will usually be set by the photometric errors. Also, unlike parameteric methods, the method doesn't necessarily require an IMF to be fully sampled by the population, since the probabilities are taken as an integral over the whole isochrone. Therefore, the method will not be as sensitive to small number statistics and will be more reliable for datasets containing fewer stars.

We have tested the method extensively using synthetic and real data for both simple and complex stellar populations. We have shown that the method is relatively robust against most systematics, including background contamination, HB morphology, IMF and completeness. Unresolved binaries are the only systematic effect that may have a significant effect on the recovered star formation history. Unlike the synthetic CMD method, which can include a binary fraction in the computation of elemental CMDs, isochrones only model single stars. In the star formation history solution, binaries are seen as an additional young metal rich populations, which in many cases, such as Carina, are separate from the main star formation events. A fully consistent way of treating unresolved binaries is beyond the scope of this paper, but it may be possible to correct for binaries if they can be isolated and identified in SFH solution. Since binaries will only affect the MS, in certain situations one indicator that the isochrone is not genuinely part of the solution will be the absence of post-MS stars in the CMD.

One of the most promising aspects of the method is that it is easily extended to datasets where there are more than two magnitude measurements per star. The probability function can be adapted to include multiple magnitudes, allowing all the information available for each star in the CMD to be used to constrain the star formation history. Another possibility is to derive the star formation history of the data using different colour combinations. Analysis of the separate probabilities for the stars can then highlight inconsistencies between the isochrones in different passbands and can possibly be used to test stellar evolution models.

## ACKNOWLEDGMENTS

We thank J. Hartman for the M 37 data. We acknowledge the Carina Project for sending us the optical catalog in electronic form. We thank the referee for a report that improved the content and presentation of this paper. EES was supported by a studentship grant from STFC.

## REFERENCES

- Aparicio, A., Gallart, C., 1995, AJ, 110, 2105
- Aparicio, A., Hidalgo, S. L., 2009, AJ, 138, 558
- Bailyn, C. D., 1995, ARA&A, 33, 133
- Bedin, L. R., King, I. R., Anderson, J., Piotto, G., Salaris, M., Cassisi, S., Serenelli, A., 2008, ApJ, 678, 1279
- Benedict, G. F., McArthur, B. E., Feast, M. W., Barnes, T. G., Harrison, T. E., Bean, J. L., Menzies, J. W., Chaboyer, B., Fossati, L., Nesvacil, N., Smith, H. A., Kolenberg, K., Laney, C. D., Kochukhov, O., Nelán, E. P.,

- Shulyak, D. V., Taylor, D., Freedman, W. L., 2011, *AJ*, 142, 187
- Bono, G., Stetson, P. B., Walker, A. R., Monelli, M., Fabrizio, M., Pietrinferni, A., Brocato, E., Buonanno, R., Caputo, F., Cassisi, S., Castellani, M., Cignoni, M., Corsi, C. E., Dall’Ora, M., Degl’Innocenti, S., François, P., Ferraro, I., Iannicola, G., Nonino, M., Moroni, P. G. P., Pulone, L., Smith, H. A., Thiévenin, F., 2010, *PASP*, 122, 651
- Brogaard, K., Bruntt, H., Grundahl, F., Clausen, J. V., Frandsen, S., Vandenberg, D. A., Bedin, L. R., 2011, *A&A*, 525, A2
- Buonanno, R., Corsi, C. E., Buzzoni, A., Cacciari, C., Ferraro, F. R., Fusi Pecci, F., 1994, *A&A*, 290, 69
- Carney, B. W., 1996, *PASP*, 108, 900
- Carney, B. W., Latham, D. W., Laird, J. B., Grant, C. E., Morse, J. A., 2001, *AJ*, 122, 3419
- Charbonneau, P., 1995, *ApJS*, 101, 309
- Cordier, D., Pietrinferni, S., Cassisi, M., Salaris, M., 2007, *AJ*, 133, 468
- de Boer, T. J. L., Tolstoy, E., Hill, V., Saha, A., Starkenberg, E., Lemasle, B., Irwin, M. J., Battaglia, G., 2012, *A&A*, 539, A103
- Dolphin, A. E., 2002, *MNRAS*, 332, 91
- Fabrizio, M., Merle, T., Thevenin, F., Nonino, M., Bono, G., Stetson, P. B., Ferraro, I., Iannicola, G., Monelli, M., Walker, A. R., Buonanno, R., Caputo, F., Corsi, C. E., Dall’Ora, M., Degl’Innocenti, S., François, P., Gilmozzi, R., Marconi, M., Pietrinferni, A., Prada Moroni, P. G., Primas, F., Pulone, L., Ripepi, V., Romaniello, M., 2012, *PASP*, 124, 519
- Harris, J., Zaritsky, D., 2001, *ApJS*, 136, 25
- Hartman, J. D., Gaudi, B. S., Holman, M. J., McLeod, B. A., Stanek, K. Z., Barranco, J. A., Pinsonneault, M. H., Meibom, S., Kalirai, J. S., 2008, *AJ*, 675, 1233
- Hernandez, X., Valls-Gabaud, D., Gilmore, G., 1999, *MNRAS*, 304, 705
- Hernandez, X., Gilmore, G., Valls-Gabaud, D., 2000, *MNRAS*, 317, 831
- Hernandez, X., Valls-Gabaud, D., 2008, *MNRAS*, 383, 1603
- Hurley-Keller, D., Mateo, M., Nemec, J., 1998, *AJ*, 115, 1840
- Kalirai, J. S., Ventura, P., Richer, H. B., Fahlman, G. G., Durrell, P. R., D’Antona, F., Marconi, G., 2001, *AJ*, 122, 3239
- Kalirai, J. S., Richer, H. B., Reitzel, D., Hansen, B. M. S., Rich, R. M., Fahlman, G. G., Gibson, B. K., & von Hippel, T., 2005, *ApJ*, 618, L123
- Koch, A., Grebel, E. K., Wyse, R. F. G., Kleyna, J. T., Wilkinson, M. I., Harbeck, D. R., Gilmore, G. F., Evans, N. W., 2006, *AJ*, 131, 895
- Koch, A., Grebel, E. K., Gilmore, G. F., Wyse, R. F. G., Kleyna, J. T., Harbeck, D. R., Wilkinson, M. I., Evans, N. W., 2008, *AJ*, 135, 1580
- Lemasle, B., Hill, V., Tolstoy, E., Venn, K. A., Shetrone, M. D., Irwin, M. J., de Boer, T. J. L., Starkenburg, E., Salvatore, S., 2012, *A&A*, 538, A100
- Michalewicz, Z., Janikow, C. Z., 1991, in *ICGA*, 151-157
- Mighell, K. J., 1997, *AJ*, 114, 1458
- Monelli, M., Pulone, L., Corsi, C. E., Castellani, M., Bono, G., Walker, A. R., Brocato, E., Buonanno, R., Caputo, F., Casettani, V., Dall’Ora, M., Marconi, M., Nonino, M., Ripepi, V., Smith, H. A., 2003, *AJ*, 126, 218
- Olsen, K. A. G., Blum, R. D., Rigault, F., 2003, *AJ*, 136, 452
- Pietrinferni, A., Cassisi, S., Salaris, M., Castelli, F., 2004, *ApJ*, 612, 168
- Piotto, G., De Angeli, F., King, I. R., Djorgovski, S. G., Bono, G., Cassisi, S., Meylan, G., Recio-Blanco, A., Rich, R. M., Davies, M. B., 2004, *AJ*, 604, 109
- Rizzi, L., Held, E. V., Bertelli, G., Saviane, I., 2003, *ApJ Let.*, 589, 85
- Salaris, M., Weiss, A., Percival, S. M., 2004, *A&A*, 414, 163
- Salaris, M., Serenelli, A., Weiss, A., Bertolami, M. M., 2009, *ApJ*, 692, 1013
- Sills, A., Pinsonneault, M. H., Terndrup, D. M., 2000, *ApJ*, 534, 335
- Shetrone, M., Venn, K. A., Tolstoy, E., Primas, F., Hill, V., Kaufer, A., 2003, *AJ*, 125, 684
- Smecker-Hane, T. A., Stetson, P. B., Hesser, J. E., Vandenberg, D. A., 1996, *ASPC*, 98, 328, *From Stars to Galaxies: the Impact of Stellar Physics on Galaxy Evolution*, ed. C. Leitherer, U. Fritze-von-Alvensleben, & J. Huchra
- Stephens, A. W., Frogel, J. A., Freedman, W., Gallart, C., Jablonka, P., Ortolani, S., Renzini, A., Rich, R. M., Davies, R., 2001, *AJ*, 121, 2584
- Stetson, P. B., Bruntt, H., Grundahl, F., 2003, *PASP*, 115, 413
- Tolstoy, E., Saha, A., 1996, *ApJ*, 462, 672
- Tolstoy, E., Venn, K. A., Shetrone, M., Primas, F., Hill, V., Kaufer, A., Szeifert, T., 2003, *AJ*, 125, 707
- Vergely, J.-L., Köppen, J., Egret, D., Bienaymé, O., 2002, *A&A*, 390, 917